Ultralow noise C + L wideband WDM-IMDD transmission at 18 × 112 Gbps by using hybrid second-order distributed Raman and first-order lumped Raman amplification

WEIYU ZHANG,[1] JIANGBING DU,[1,2,*] ![ORCID] MINGMING TAN,[3] ![ORCID] AND ZUYUAN HE[1,2]

[1] *State Key Laboratory of Advanced Optical Communication Systems and Networks, Department of Electronic Engineering, Shanghai Jiao Tong University, Shanghai 200240, China*
[2] *Peng Cheng Laboratory, Shenzhen 518055, China*
[3] *Aston Institute of Photonic Technologies, Aston University, Birmingham B4 7ET, UK*
[*] *dujiangbing@sjtu.edu.cn*

Abstract: We experimentally investigated and demonstrated an ultralow noise hybrid amplifier that combines second-order distributed Raman amplifier (DRA) and first-order lumped Raman amplifier (LRA) in a cascaded approach. This approach allows for the reutilization of pump light from the LRA as the seed light in the second-order DRA, and simultaneous full-band dispersion compensation is realized by using dispersion compensation fiber in the LRA. This approach also supports broadband gain flattening based on the separated DRA and LRA configuration. The transmission application of the proposed amplifier was investigated using a set of 10 external cavity lasers (ECLs) in the C-band and 8 ECLs in the L-band. Ranging from 1531.12 nm to 1595.49 nm across C + L band, the proposed hybrid amplifier gives a maximum on-off gain of 27.2 dB and an average gain of 23.4 dB, with an extremely low effective noise figure (NF) of lower than -2.9 dB. Intensity modulation direct detection (IMDD) signal transmission is carried out at two different data rates across these 18 wavelengths in the C + L band: (1) 56 Gbps/λ PAM-4 signal; (2) 112 Gbps/λ PAM-4 signal. The results show that the error free transmissions are demonstrated over 101.6 km EX2000 fiber using both signals with 7% HD-FEC and 20% SD-FEC, respectively.

1. Introduction

The relentless pursuit of larger capacity and longer transmission distances is always the key driving force for the development of optical fiber communications [1]. To enlarge the capacity of optical fiber communication systems, fully utilizing the low-loss transmission window of single-mode fibers presents a cost advantage over space-division multiplexing (SDM) techniques due to its ability to leverage the already deployed infrastructure [2,3]. In order to enable optical transmission through the untapped fiber windows, it is necessary to design and develop optical amplifiers that support optical amplification in these spectral bands [4,5]. Moreover, achieving longer unrepeatered transmission distances imposes higher requirements on the noise figure and gain capability of optical amplifiers [6].

A plethora of experiments have demonstrated the use of various technological approaches for ultra-wideband optical amplifiers [7–16]. For instance, by employing different types of doped fibers as the amplification medium, rare-earth-doped fiber amplifiers can achieve broadband amplification that covers different wavelength ranges [7–9]. Semiconductor optical amplifiers (SOA) also serve as an attractive solution for UWB amplification, as evidenced by experiments showcasing amplification bandwidths exceeding 100 nm [10,11]. In addition, experiments utilizing cascaded lumped Raman amplifiers (LRA) for UWB optical transmission have shown

that by employing multi-pump configurations, amplification bandwidths over 200 nm can be achieved [12–15]. Notably, UWB coherent transmissions, covering the O-, E-, S-, C-, and L-bands has been successfully demonstrated with 195 nm amplification bandwidth [15].

The realization of ultralow noise amplification, which effectively suppresses the degradation of the optical signal-to-noise ratio (OSNR) during transmission, is commonly achieved through the utilization of distributed Raman amplifiers (DRA) [6]. However, it is necessary to combine them with other amplifiers when the transmission link experiences significant loss. In certain experiments, the combination of DRA with remote optically-pumped amplifiers (ROPA) or SOA has enabled the extension of unrepeatered transmission distances to over 400 km [16–18]. Therefore, with the consideration of UWB amplification, combined amplification configuration is highly necessary and issues including low-noise, high gain and power consumption still need investigation.

In this study, we propose a hybrid Raman amplifier (HRA), which is composed of cascaded second-order DRA and LRA. The effective noise figure (NF) of cascaded optical amplifiers primarily depends on the first-stage optical amplifier [19]. By incorporating the LRA in cascade after the DRA, the dual-stage HRA achieves an effective NF that approximates that of the DRA. Furthermore, this cascaded structure enables the injection of residual pump power from the LRA into the transmission fiber, serving as lower-order pump seed for higher-order distributed Raman amplification. This enhances the energy utilization efficiency of the pump. The studies mentioned in [20,21] indicate that higher-order DRA exhibits lower NF and higher gains due to their more pronounced distributed amplification characteristics. In addition, all pumps of the dual-stage HRA are employed in the backward pumping configuration, minimizing the impact of relative intensity noise (RIN). The experimental results indicate a maximum on-off gain of 27.2 dB and an average gain of 23.4 dB for the proposed HRA. It is worth noting that the effective NF of this dual-stage HRA is below -2.9 dB, which is close to the effective NF of the second-order DRA that is below -4.4 dB. By utilizing a proper distance of dispersion compensating fiber (DCF) as the gain medium in the LRA, this amplifier can be employed to compensate for the accumulated dispersion of optical signals through transmission link. Employing the dual-stage HRA without the need for additional dispersion compensation measures, we realized WDM transmission of 56 Gbps/λ PAM-4 signals below the 7% overhead hard-decision forward error correction (HD-FEC) bit error rate (BER) threshold, and 112 Gbps/λ PAM-4 under the 20% overhead soft-decision forward error correction (SD-FEC) BER threshold, across these 18 wavelengths in the C + L band.

2. Dual-stage hybrid Raman amplification

The dual-stage HRA is characterized using an experimental setup as shown in Fig. 1. The input optical signals were generated by 10 ECLs in the C-band and 8 ECLs in the L-band. They were coupled into the single mode fiber (SMF) EX2000 together through an arrayed waveguide grating (AWG). The frequency range of the C-band ECLs starts at 192.2 THz (1559.79 nm) with a channel spacing of 400 GHz and ends at 195.8 THz (1531.12 nm). The L-band ECLs have a frequency range starting at 187.9 THz (1595.49 nm) with a channel spacing of 300 GHz and ending at 190.0 THz (1577.86 nm). We conducted experimental tests using a total signal power of 15.5 dBm and 23.2 dBm (equivalent to approximately 3 dBm and 11 dBm per channel, respectively). The total power of 15.5 dBm was used to test the gain and (effective) NF of the DRA and LRA. The total power of 23.2 dBm was used to test the gain saturation of the dual-stage LRA and observe the power transfer from shorter-wavelength signals to longer-wavelength signals caused by inter-channel stimulated Raman scattering (ISRS). An optical isolator (ISO) was implemented to prevent the backscattered portion of Rayleigh scattering (RS) of the optical signals from entering the ECLs. The lengths of the EX2000 and the dispersion compensating fiber (DCF) are 101.6 km and 15.7 km, respectively. The three wavelength division multiplexers (WDMs) were

utilized in the dual-stage HRA. WDM1 coupled the pumps of the DRA into the EX2000, while WDM3 coupled the pumps of the LRA into the DCF. WDM2 coupled the residual pump power from the LRA into the EX2000, serving as the first-order pump for the second-order DRA. Two optical spectrum analyzers (OSAs) were used for the experiment, with OSA1 primarily utilized for testing DRA, while OSA2 was primarily employed for testing LRA and dual-stage HRA. A total of 5 pumps at wavelengths of 1360, 1425, 1465, 1480 and 1500 nm, with pump power values of 2180, 421, 237, 56 and 327 mW respectively, were used for C + L band signal amplification.
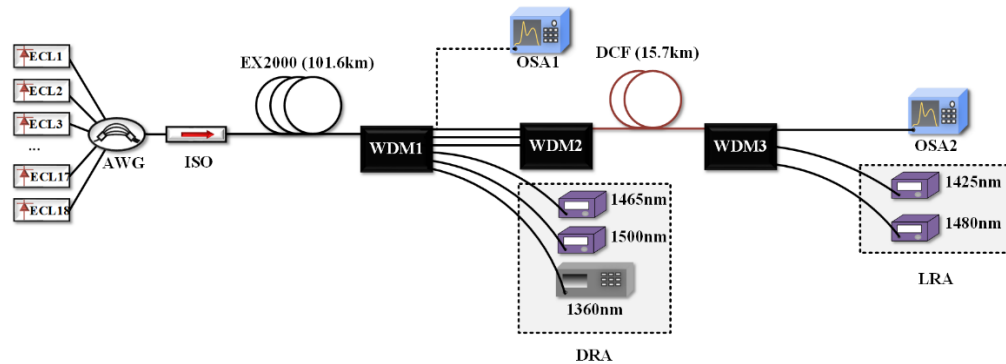

Fig. 1. Schematic of the dual-stage HRA.

The unamplified optical spectrum at the output of DCF, and the optical spectrum amplified by the dual-stage HRA at the output of DCF are shown in Fig. 2(a) and 2(b). From Fig. 2(b), it can be observed that the amplified spontaneous emission (ASE) power in the C-band is higher than that in the L-band. This is due to the smaller frequency distance between the pumps and the C-band optical signals, resulting in a stronger stimulated Raman scattering (SRS) thermal noise and therefore generating higher ASE power compared to the L-band [12]. Besides, the optical spectrum at the output of DCF with dual-stage HRA exhibits approximately 6 dB of fluctuation in optical power across these 18 wavelengths in the C + L band. This is due to the limitations imposed by the maximum power and fixed wavelength of our pumps, resulting in non-uniform gain provided by the dual-stage HRA. By employing additional pumps and machine learning based inverse optimization methods for pump power configuration, it is possible to achieve a gain from the dual-stage HRA that better aligns with our requirements [22].
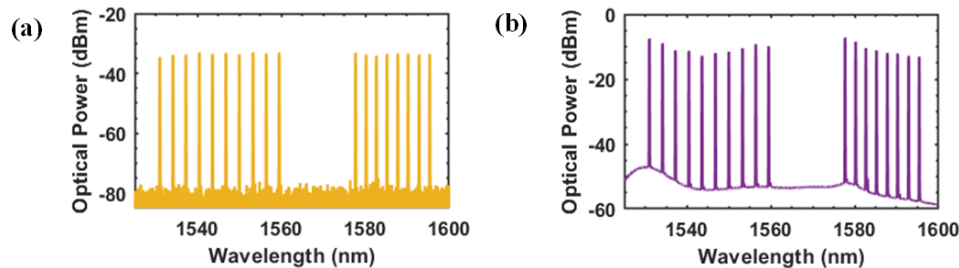

Fig. 2. The optical spectrum of a) output from DCF without amplification b) output from DCF with amplification by dual-stage HRA.

The total loss of the transmission link (including EX2000, ISO, DCF, and all WDM) and the on-off gain of the dual-stage HRA at different total signal power levels are shown in Fig. 3(a) and (b). From Fig. 3(a), it can be observed that the total loss of the transmission link ranges from 32.5 dB to 31.3 dB. Moreover, we can observe that there is a power transfer from shorter

wavelengths to longer wavelengths caused by the impact of ISRS. Compared to the low-power input scenario, at high power levels, the loss at shorter wavelengths increased by 0.5 dB, while the loss at longer wavelengths decreased by 0.3 dB. Indeed, this implies the ISRS contribution varies by approximately 0.8 dB between the ends of the spectrum we investigated. From Fig. 3(b), it can be observed that at a total signal power of 15.5 dBm, the highest on-off gain of the dual-stage HRA is 27.2 dB, the lowest on-off gain is 21.3 dB, and the average on-off gain is 23.4 dB. When the total signal power increases to 23.2 dBm, the highest on-off gain of the dual-stage HRA is 24.3 dB, the lowest on-off gain is 17.8 dB, and the average on-off gain is 19.8 dB. Consequently, it is evident that our dual-stage HRA experiences a decrease of approximately 3 dB in on-off gain at a high input power of 23.2 dBm but still maintains a relatively high on-off gain close to 20 dB. At the shorter wavelength end of the on-off gain spectrum, the on-off gain reaches its peak, indicating that our dual-stage HRA possesses a notable capability to amplify optical signals of even shorter wavelengths.
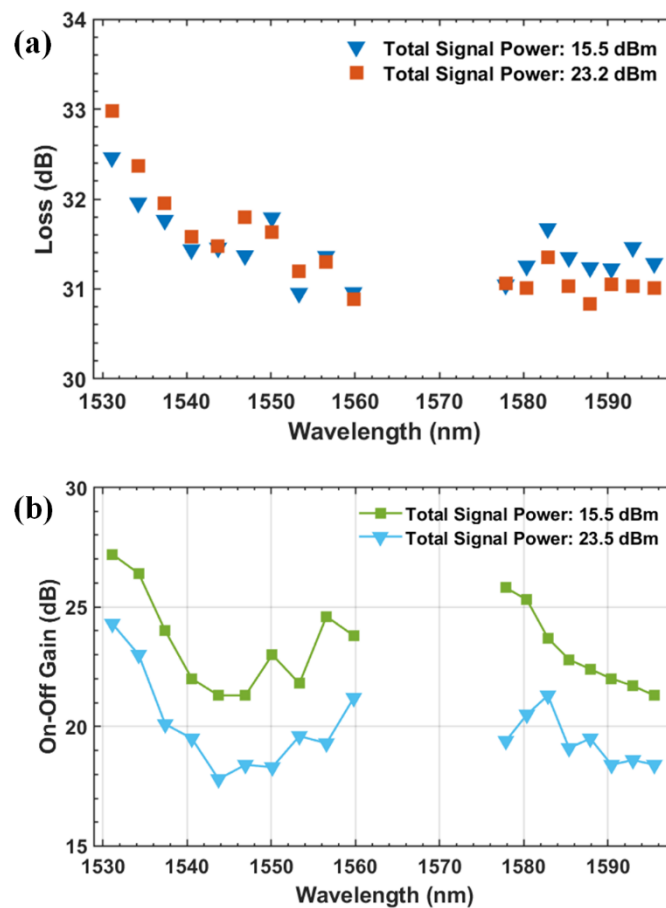

Fig. 3. a) The total loss of the transmission link at different total signal power levels. b) The on-off gain of the dual-stage HRA at different total signal power levels.

The on-off gain and effective NF of DRA, the on-off gain and NF of LRA, the effective NF of dual-stage HRA, as well as the effective NF of dual-stage HRA calculated from the equation of cascaded amplifier total NF, and the OSNR at the output of SMF and DCF, at the total signal
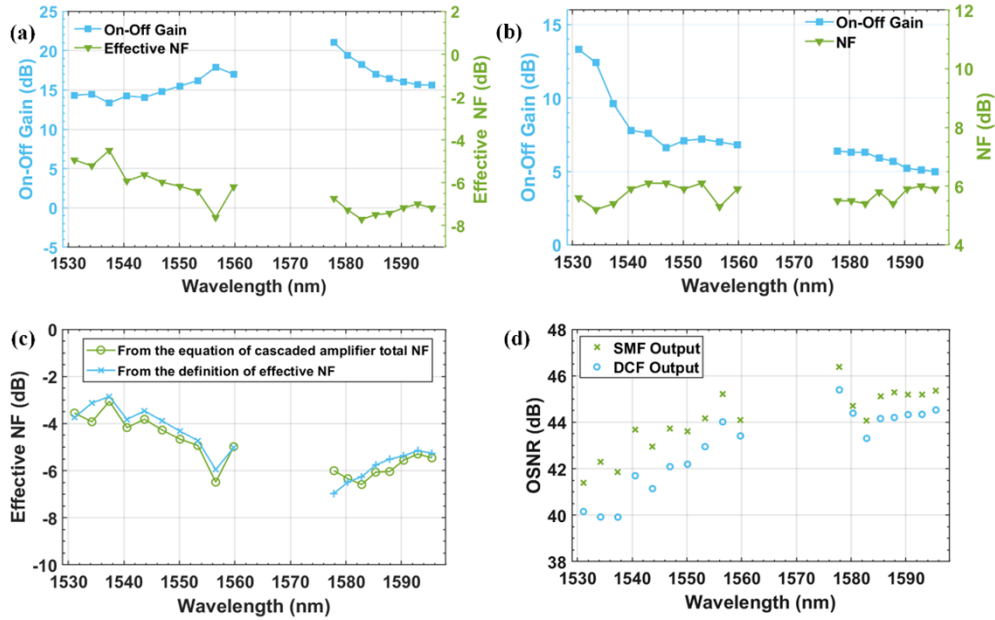
Fig. 4. a) The on-off gain and effective NF of DRA. b) The on-off gain and NF of LRA. c) The effective NF of dual-stage HRA, as well as the effective NF of dual-stage HRA calculated from the equation of cascaded amplifier total NF. d) Output OSNR of SMF and DCF.

power of 15.5 dBm are shown in Fig. 4(a)–(d). The NF and effective NF are defined as [19]:

$$NF = \frac{1}{G}\left(1 + \frac{P_{ASE}}{E_{ph}B_0}\right) \tag{1}$$

where E_{ph} is the signal photon energy, and P_{ASE} is the ASE noise power measured in a bandwidth B_0. For DRA, G represents the on-off gain. For LRA, G represents the net gain. And for dual-stage HRA, G represents the product of the on-off gain of DRA and the net gain of LRA. The effective NF of dual-stage HRA can also be calculated based the effective NF of DRA and the NF of LRA, by using the equation for the total NF of cascaded amplifiers given in [6]:

$$NF_{total} = NF_1 + \frac{NF_2 - 1}{G_1} \tag{2}$$

Where NF_1 is the NF of the first-stage amplifier, NF_2 is the NF of the second-stage amplifier, and G_1 is the gain of the first-stage amplifier. For our dual-stage HRA the first-stage amplifier is the DRA and the second-stage amplifier is the LRA. From Fig. 4(a), it can be observed that the effective NF of DRA is higher at shorter wavelengths compared to longer wavelengths. In Fig. 4(b), LRA exhibits higher gain in the C-band than L-band, which helps to balance the stronger amplification capability of DRA in the L-band of than C-band. From Fig. 4(c), it can be observed that the effective NF of dual-stage HRA obtained through two different methods are very close and exhibit higher values in the C-band, which aligns with the conclusion drawn from Fig. 2(b) that the ASE power is higher in the C-band. The reason behind this phenomenon, as mentioned earlier, is attributed to the fact that the pumps is closer to the C-band optical signal in the frequency domain. This will generate stronger thermal noise, resulting in a higher ASE noise. Furthermore, power transfer resulting from SRS causes pump-to-pump interactions, leading to shorter-wavelength pump light being unable to penetrate deep into the fiber, resulting in higher

effective NF in the C-band. Using more higher-order pumps can compensate for the energy loss of shorter- wavelength pumps, allowing them to penetrate deeper into the fiber and reducing the effective NF in the C-band. This is due to the more uniform distribution of Raman gain within the optical fiber, resulting in smaller fluctuations in optical power of the optical signal and hence, yielding a lower NF. Figure 4(c) demonstrates that the effective NF of the dual-stage HRA is close to that of the DRA. This indicates that our cascaded structure effectively mitigates the impact of the high NF associated with the lumped LRA. The OSNR results shown in Fig. 4(d) confirm this observation, as the degradation in OSNR caused by the LRA is kept under control at approximately 1~2 dB.

3. WDM IMDD transmission with dual-stage hybrid Raman amplifier

Since the receiver in the IMDD transmission system can only captures the intensity component of the optical signal, digital signal processing-based electronic dispersion compensation methods are not suitable for IMDD transmission systems. The dispersion compensation characteristics of our amplifier hold greater value in IMDD transmission systems, which is why we opted for the IMDD system for validating the transmission performance. IMDD transmission was carried out using the setup illustrated in Fig. 5. The ECLs were individually extracted from the shortest to the longest wavelengths for transmission quality testing. Apart from the tested ECL, the remaining 17 ECLs were coupled into SMF through the AWG to simulate optical interactions between WDM channels in the role of WDM Grid. We adjusted the power of the tested ECL and compensated for the insertion loss (IL) of the modulator to ensure that the optical power of all ECLs entering the SMF was approximately equal, around 3 dBm. The slightly higher launch power is aimed at aligning the total launch power with that of dense wavelength-division multiplexing systems. This may result in our single-channel launch power being higher than the optimal launch power. The Keysight M8192A was employed as a digital-to-analog converter (DAC) to generate electrical signals, which were then applied to the modulator. The sampling rate used was 64 GSa/s. The optical tunable filter (OTF) Santec OTF-970 was utilized to select the desired wavelength of the optical signals. An erbium-doped fiber amplifier (EDFA) capable of operating in the C + L band was employed to compensate for the IL of the OTF. The optical signals were received using a photodetector (PD) with a bandwidth of 50 GHz and a real-time oscilloscope (Keysight, DSOZ592A) with a sampling rate of 80 GSa/s (33 GHz analog bandwidth). The pump configuration remains the same as in the amplification experiment. Offline digital signal processing (DSP) techniques were also applied to estimate the BER, following the flowchart illustrated in Fig. 5.
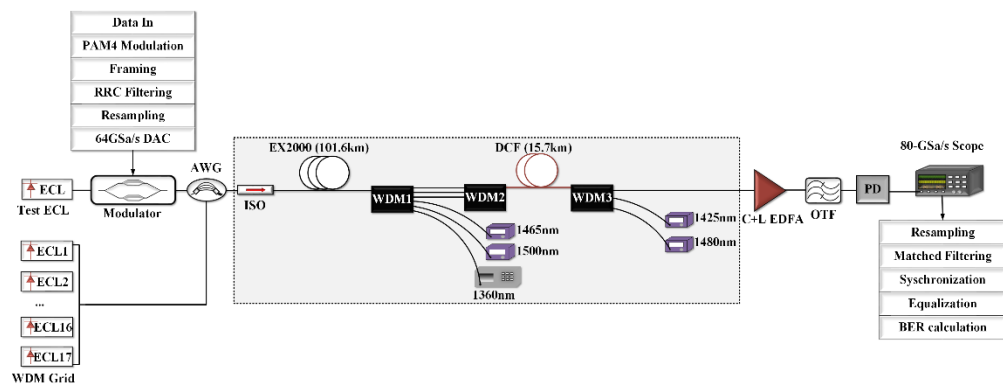

Fig. 5. The schematic of the transmission experiment with dual-stage HRA amplification.

In order to obtain more general experimental results, we transmitted PAM-4 signals at both 56 Gbps and 112 Gbps data rate for each wavelength. Additionally, a comparison was made between the transmission results under back-to-back (B2B) conditions and those for 101.6 km transmission with dual-stage HRA amplification. The WDM channels were numbered from 1 to 18 according to their wavelengths, starting from the shortest wavelength and proceeding to the longest wavelength.

The experimental results for the data rate of 56 Gbps are shown in Fig. 6. It can be observed that compared to the B2B scenario, the transmission over 101.6 km exhibits a higher BER. However, it remains below the 7% HD-FEC BER threshold (3.8×10^{-3}) with the dual-stage HRA amplification. The experimental results for the transmission rate of 112 Gbps are depicted in the Fig. 7. Under B2B conditions, the BER is below the 7% HD-FEC BER threshold. With the transmission over 101.6 km, there is an increase in the BER, but it remains below the 20% SD-FEC BER threshold (2.4×10^{-2}) with the dual-stage HRA amplification. The results of our experiments demonstrate that our dual-stage HRA can compensate for accumulated dispersion during the optical signal transmission process by appropriately selecting the length of the DCF. It achieves this without the need for any other dispersion compensation measures, including electronic dispersion compensation (EDC). Additionally, we can observe that the BER in the L-band is slightly lower than the BER in the C-band. This can be reasonably explained by the fact that the lower effective NF of the dual-stage HRA in the L-band results in a higher OSNR. By splitting the second-order DRA into two stages, it is possible to suppress power transfer between pumps and improve these results [23].
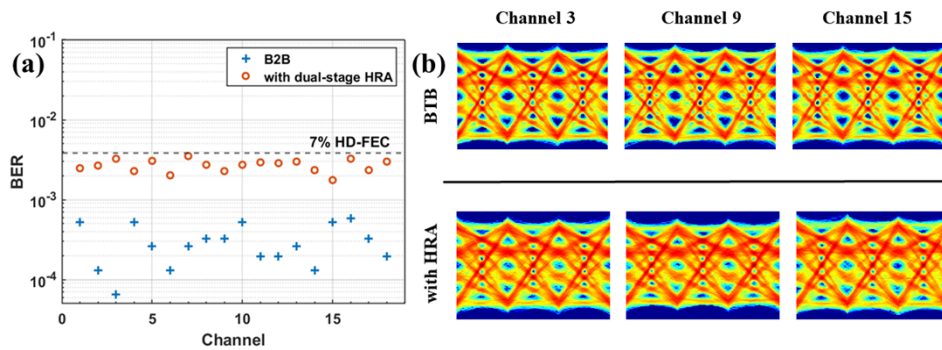

Fig. 6. a) The BER of 18 channels at a data rate of 56 Gps/λ. b) The eye diagrams for channel 3, channel 9, and channel 15 at a data rate of 56 Gps/λ.
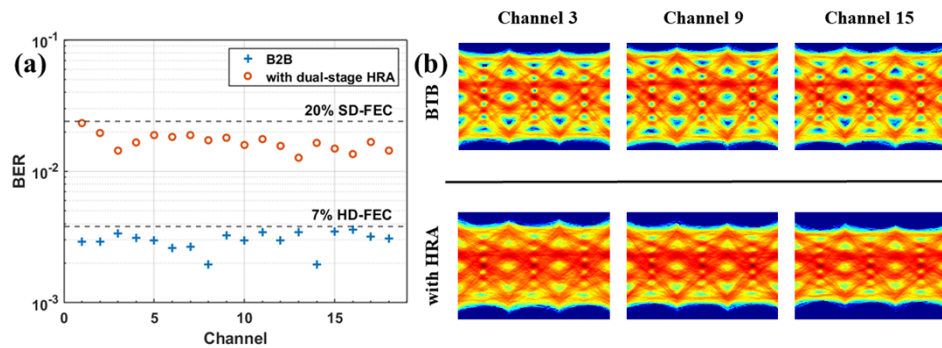

Fig. 7. a) The BER of 18 channels at a data rate of 112 Gps/λ. b) The eye diagrams for channel 3, channel 9, and channel 15 at a data rate of 112 Gps/λ.

4.　Conclusions

We experimentally demonstrated the gain and noise performance of the proposed dual-stage HRA, as well as conducted Wavelength-division multiplexing IMDD transmission experiments with the dual-stage HRA amplification. The dual-stage HRA achieves a maximum on-off gain of 27.2 dB and an average gain of 23.4 dB. Moreover, its effective NF is close to that of the second-order DRA, being lower than -2.9 dB. This indicates that the dual-stage HRA can enhance the gain capability of the DRA while retaining its ultralow noise characteristics. The employing of higher-order DRA also allows for the utilization of residual pump power from the LRA, thereby improving the energy efficiency of the Raman pumping process. The transmission experiments were conducted using PAM-4 modulation format, achieving a data rate of 112 Gbps/λ. This demonstrates that the dual-stage HRA can compensate for optical power loss during the transmission process. Besides, the conclusion that the use DCF as the gain medium in the LRA effectively compensates for signal dispersion can be derived from the experimental results. For coherent transmission systems employing electronic dispersion compensation techniques, it is possible to replace the DCF with high nonlinearity fiber to achieve higher gain. Based on our experiments, the dual-stage HRA can be deployed to provide broadband, high-gain, and ultralow noise amplification to compensate for link losses in wideband ultralong-haul transmissions. Finally, higher-order pumps and additional pumps can further enhance the performance of the dual-stage HRA, offering even better amplification capabilities.

Disclosures. The authors declare no conflicts of interest.

Data availability. Data underlying the results presented in this paper are not publicly available at this time but may be obtained from the authors upon reasonable request.

References

1. P. J. Winzer, D. T. Neilson, and A. R. Chraplyvy, "Fiber-optic Transmission and Networking: The Previous 20 and the next 20 Years [Invited]," Opt. Express **26**(18), 24190–24239 (2018).
2. Q. Zhuge, X. Chen, D. V. Plant, and W. Shieh, "Feature Issue Introduction: Ultra-wideband Optical Communications," Opt. Express **30**(8), 13591–13593 (2022).
3. C. Papapavlou, K. Paximadis, and G. Tzimas, "Design and Analysis of a New SDM Submarine Optical Network for Greece," in *2021 International Conference on Information, Intelligence, Systems & Applications (IISA)* (2021), pp. 1–8.
4. J. Renaudier, A. Napoli, M. Ionescu, C. Calo, G. Fiol, V. Mikhailov, W. Forysiak, N. Fontaine, F. Poletti, and P. Poggiolini, "Devices and Fibers for Ultrawideband Optical Communications," Proc. IEEE **110**(11), 1742–1759 (2022).
5. L. Rapp and M. Eiselt, "Ultra-Wideband Amplification Strategies," in *2021 IEEE Photonics Society Summer Topicals Meeting Series (SUM)* (2021), pp. 1–2.
6. W. S. Pelouch, "Raman Amplification: An Enabling Technology for Long-Haul Coherent Transmission Systems," J. Lightwave Technol. **34**(1), 6–19 (2016).
7. J. Mirza, S. Ghafoor, N. Habib, F. Kanwal, and K. K. Qureshi, "Performance evaluation of praseodymium doped fiber amplifiers," Opt. Rev. **28**(6), 611–618 (2021).
8. Y. Wang, N. K. Thipparapu, D. J. Richardson, and J. K. Sahu, "Ultra-Broadband Bismuth-Doped Fiber Amplifier Covering a 115-nm Bandwidth in the O and e Bands," J. Lightwave Technol. **39**(3), 795–800 (2021).
9. B. J. Puttnam, R. S. Luís, G. Rademacher, M. Mendez-Astudillio, Y. Awaji, and H. Furukawa, "S-, C- and L-band transmission over a 157 nm bandwidth using doped fiber and distributed Raman amplification," Opt. Express **30**(6), 10011–10018 (2022).
10. J. Renaudier, A. C. Meseguer, A. Ghazisaeidi, P. Tran, R. R. Muller, R. Brenot, A. Verdier, F. Blache, K. Mekhazni, B. Duval, H. Debregeas, M. Achouche, A. Boutin, F. Morin, L. Letteron, N. Fontaine, Y. Frignac, and G. Charlet, "First 100-nm Continuous-Band WDM Transmission System with 115Tb/s Transport over 100 km Using Novel Ultra-Wideband Semiconductor Optical Amplifiers," in *2017 European Conference on Optical Communication ECOC* (2017), pp. 1–3.
11. A. Arnould, R. Ryf, H. Chen, M. Achouche, J. Renaudier, A. Ghazisaeidi, D. L. Gac, P. Brindel, M. Makhsiyan, K. Mekhazni, F. Blache, N. Fontaine, and D. Neilson, "103 nm Ultra-Wideband Hybrid Raman/SOA Transmission Over 3 × 100 km SSMF," J. Lightwave Technol. **38**(2), 504–508 (2020).

12. S. Liang, S. Jain, L. Xu, K. R. H. Bottrill, N. Taengnoi, M. Guasoni, P. Zhang, M. Xiao, Q. Kang, Y. Jung, P. Petropoulos, and D. J. Richardson, "High Gain, Low Noise, Spectral-Gain-Controlled, Broadband Lumped Fiber Raman Amplifier," J. Lightwave Technol. **39**(5), 1458–1463 (2021).

13. P. Hazarika, M. Tan, A. Donodin, I. Phillips, P. Harper, and W. Forysiak, "210 nm E, S, C and L Band Multistage Discrete Raman Amplifier," in *2022 Optical Fiber Communication Conference (OFC)* Tu3E.2 (2022).

14. A. Donodin, P. Hazarika, M. Tan, V. Dvoyrin, M. Patel, I. Phillips, P. Harper, S. Turitsyn, and W. Forysiak, "195-nm Multi-band amplifier enabled by bismuth-doped fiber and discrete Raman amplification," in *2022 European conference of optical communication (ECOC)* Th2A.1 (2022).

15. P. Hazarika, M. Tan, A. Donodin, S. Noor, I. Phillips, P. Harper, J. S. Stone, M. J. Li, and W. Forysiak, "E-, S-, C- and L-band Coherent Transmission with a Multistage Discrete Raman Amplifier," Opt. Express **30**(24), 43118–43126 (2022).

16. J. C. S. S. Januario, A. Chiuchiarelli, S. M. Rossi, J. H. Cruz, J. D. Reis, C. Mornatta, A. Festa, and A. C. Bordonalli, "System Design for High-Capacity Unrepeatered Optical Transmission," J. Lightwave Technol. **37**(4), 1246–1253 (2019).

17. A. Ghazisaeidi, A. Arnould, M. Ionescu, V. Aref, H. Mardoyan, S. Etienne, M. Duval, C. Bastide, H. Bissessur, and J. Renaudier, "99.35 Tb/s Ultra-wideband Unrepeated Transmission over 257 km Using Semiconductor Optical Amplifiers and Distributed Raman Amplification," J. Lightwave Technol. **40**(21), 7014–7019 (2022).

18. J. Wu, J. Xu, Q. Hu, J. Yu, J. Liu, Q. Luo, W. Wang, L. Huang, C. Huang, H. Long, S. Sun, M. Duan, M. Xiang, and G. He, "Unrepeatered Transmission of Single-Carrier 800Gb/s over 404 km with Commercial Transceiver and Enhanced ROPA System," in *2021 Optical Fiber Communications Conference and Exhibition (OFC)* (2021) pp. 1–3.

19. J. Bromage, "Raman amplification for fiber communications systems," J. Lightwave Technol. **22**(1), 79–93 (2004).

20. Y. Hadjar, N. J. Traynor, and S. Gray, "Noise figure tilt reduction in ultrawide-band WDM through second-order Raman amplification," IEEE Photonics Technol. Lett. **16**(4), 1200–1202 (2004).

21. J.-C. Bouteiller, K. Brar, J. Bromage, S. Radic, and C. Headley, "Dual-order Raman Pump," IEEE Photonics Technol. Lett. **15**(2), 212–214 (2003).

22. Y. Chen, J. Du, Y. Huang, K. Xu, and Z. He, "Intelligent Gain Flattening in Wavelength and Space Domain for FMF Raman Amplification by Machine Learning Based Inverse Design," Opt. Express **28**(8), 11911–11920 (2020).

23. P. Hazarika, M. Tan, A. Donodin, M. Patel, I. Phillips, P. Harper, and W. Forysiak, "Ultra-wideband Discrete Raman Amplifier Optimization for Single-span S-C-L-band Coherent Transmission Systems," Opt. Lett. **47**(24), 6472–6475 (2022).